Available online at www.sciencedirect.com
ScienceDirect
International Journal of Thermal Sciences 47 (2008) 848–857
International Journal of Thermal Sciences
www.elsevier.com/locate/ijts

Exact analytical results for the thermosolutal MHD Marangoni boundary layers

E. Magyari [a,*], A.J. Chamkha [b]

[a] *Institute of Building Technology, ETH Zürich, Wolfgang-Pauli-Str. 1, CH-8093 Zürich, Switzerland*
[b] *Manufacturing Engineering Department, The Public Authority for Applied Education and Training, P.O. Box 42325, Shuweikh, 70654 Kuwait*

Received 30 January 2007; received in revised form 2 July 2007; accepted 4 July 2007

Available online 8 August 2007

Abstract

The steady laminar magnetohydrodynamic (MHD) thermosolutal Marangoni convection in the presence of a uniform applied magnetic field is considered in the boundary layer approximation. It is assumed that the surface tension varies linearly with both the temperature and concentration and that the interface temperature and concentration are quadratic functions of the interface arc length x. Exact analytical solutions for the velocity, temperature and concentration boundary layers are reported. The heat and mass transfer characteristics of the flow as functions of the physical parameters of the problem are discussed in detail.

Keywords: Thermosolutal Marangoni convection; MHD; Boundary layers; Similarity solutions; Dual solutions

1. Introduction

Marangoni boundary layers are dissipative layers which may occur along liquid–liquid or liquid–gas interfaces. The surface tension gradients that are responsible for Marangoni convection can be both temperature and/or concentration gradients. The basic research work in this field was first promoted by Napolitano [1,2]. Marangoni flow induced by surface tension variations along the liquid–fluid interface causes undesirable effects in crystal growth melts in the same manner as buoyancy-induced natural convection [3,4]. These undesirable effects become dominant in the absence of buoyancy forces in the microgravity environment of space-based crystal growth experiments [4,5].

In spite of its significance and relevance in microgravity crystal growth, welding, semiconductor processing and several other fields of space science, thermosolutal Marangoni convection has not been fully explored especially regarding preliminary questions of a general and basic nature. As pointed out by Napolitano [6], the field equations in the bulk fluids do not depend explicitly on the geometry of the interface when using as coordinates the arc length (x). This, together with the other surface balance equations, introduces kinematic, thermal and pressure couplings for the flow fields in the two fluids. Napolitano and Golia [7] have shown that the fields are uncoupled when the momentum and energy resistivity ratios of the two layers and the viscosity ratio of the two fluids are much less than one. Furthermore, as shown by Napolitano and Russo [8], similarity solutions for Marangoni boundary layers exist when the interface temperature gradient varies as a power of the interface arc length (x). The power laws for all other variables, including the mean curvature, were determined. Numerical solutions were found, analyzed and discussed on Marangoni boundary layers in subsequent papers by Golia and Viviani [9,10], Napolitano et al. [11] and Pop et al. [12].

The numerous investigations of Marangoni flow in various geometries have been reviewed in the literature [13,14]. Some of the papers most relevant to this work include the order-of-magnitude analysis of Marangoni flow given by Okano et al. [15] that gave the general trends for the variation of the Reynolds number with the Grashof number, Marangoni number, and Prandtl number. Hirata and his co-workers experimentally and numerically investigated Marangoni flow for var-

* Corresponding author. Tel.: +41 44 633 28 67; fax: +41 44 633 10 41.
E-mail address: magyari@hbt.arch.ethz.ch (E. Magyari).

1290-0729/$ – see front matter
doi:10.1016/j.ijthermalsci.2007.07.004

Nomenclature

a	Parameter, Eq. (21)
$a_{1,2,3}$	Parameters, Eqs. (25)
B_0	Magnetic induction, Eq. (2)
c	Dimensional concentration, Eq. (4)
C	Dimensionless concentration, Eqs. (8)
C_0	Dimensional constant, Eq. (7b)
D	Mass diffusivity, Eq. (4)
$f'(0)$	Tangential component of the dimensionless interface velocity
$f(\eta)$	Similar stream function, Eqs. (8)
${}_1F_1$	Confluent hypergeometric function, Eqs. (44)
H	Hartmann number
L	Reference length, Eq. (14)
$\dot{m}$	Mass flow rate per unit span, Eq. (16)
M	Square of the Hartmann number H, Eq. (9)
p	Parameter, Eq. (38)
Pr	Prandtl number, $Pr = \nu/\alpha$
r	Ratio of the solutal and thermal Marangoni numbers, Eq. (13)
s	Parameter, Eq. (53)
$s_{1,2}$	Parameters, Eq. (26)
Sc	Schmidt number, $Sc = \nu/D$
T	Dimensional temperature, Eq. (3)
T_0	Dimensional constant, Eq. (7b)
u, v	x- and y-component of the dimensional velocity, respectively.
z	Independent variable, Eq. (41)
x, y	Cartesian coordinates

Greek symbols

α	Thermal diffusivity, Eq. (3)
δ_{el}	Electrical conductivity, Eq. (2)
δ	Thickness of velocity boundary layer, Eq. (33)
Δ	Discriminant, Eq. (27)
γ	Coefficients, Eq. (5)
η	Similarity independent variable, Eqs. (8)
μ	Dynamic viscosity
υ	Kinematic viscosity, $\nu = \mu/\rho$
θ	Temperature similarity variable, Eqs. (8)
ρ	Density
σ	Surface tension, Eq. (5)
ψ	Stream function, Eqs. (8)

Subscripts

T	Thermal quantity
C	Solutal quantity
0	at $\eta = 0$
∞	for $\eta \to \infty$

ious substances in geometries with flat surfaces relevant to this work [13,15,16]. Arafune and Hirata [17] presented a similarity analysis for just the velocity profile for Marangoni flow that is very similar to this derivation but the results are effectively limited to surface tension variations that are linearly related to the surface position. Slavtchev and Miladinova [18] presented similarity solutions for surface tension that varied as a quadratic function of the temperature as would occur near a minimum. Schwabe and Metzager [19] experimentally investigated Marangoni flow on a flat surface combined with natural convection in a unique geometry where the Marangoni effect and the buoyancy effect could be varied independently. Christopher and Wang [3] studied Prandtl number effects for Marangoni convection over a flat surface and presented approximate analytical solutions for the temperature profile for small and large Prandtl numbers.

Napolitano et al. [20] considered double-diffusive boundary layer along a vertical free surface. Pop et al. [12] analyzed thermosolutal Marangoni forced convection boundary layers that can be formed along the surface, which separates two immiscible fluids in surface driven flows when the Reynolds number is large enough. They derived similarity equations for the case in which an external pressure gradient is imposed and produced numerical results for these equations based on the Keller-box and superposition methods. Recently, Al-Mudhaf and Chamkha [21] reported numerical and approximate results for thermosolutal Marangoni convection along a permeable surface in the presence of heat generation or absorption and a first-order chemical reaction effects. Exact analytic solutions for this case have been reported recently by Magyari and Chamkha [22]. As mentioned by Christopher and Wang [23], for an interface with evaporation or condensation at the surface, the temperature distribution along the interface is primarily a function of the vapor temperature and the heat transfer coefficient rather than the Marangoni flow. For instance, Christopher and Wang [23] showed that the calculated temperature distribution in vapor bubble attached to a surface and in the liquid surrounding the bubble was primarily due to the heat transfer through the vapor rather than in the liquid region and the temperature variation along the surface was not linear but could be described by a power-law function. For this reason, it is assumed that both the wall temperature and solute concentration are power-law functions of the distance along the plate surface.

The application of magnetic fields is widely used in the semiconductor crystal growth industry as well as in the casting technologies to dampen the undesired convective heat and mass transport fluctuations in the melt. In the field of the growth of large diameter silicon crystals by the Czochralski (Cz) technique, steady magnetic fields are used to improve the process conditions by damping harmful temperature fluctuations in the melt as well as by controlling the oxygen distribution in the crystal [24]. Hainke et al. [24] investigated the basic interactions between magnetic fields and natural and Marangoni convections for crystal growth and alloy solidification. The influence of steady magnetic fields [25–27] as well as of rotating magnetic fields [28–31] on the buoyant flow

was analyzed intensively by using so-called convection cells filled with liquid Gallium to which different boundary conditions can be applied. In such systems, different studies can be made to select proper parameters of the magnetic field in which a beneficial effect on the crystal growth process can be expected. Witkowski and Walker [32] considered axisymmetric flow driven by Marangoni convection and rotating magnetic field in a floating-zone configuration for low Prandtl number and different Marangoni number values. Priede et al. [33] studied the theoretical aspects of thermocapillary convection in liquid metals under the influence of magnetic fields. Also, Priede et al. [34] demonstrated that a magnetic field acting on the thermocapillary flow of a low Prandtl number fluid caused the fluid to behave like a high Prandtl number fluid. This important feature was exemplified by considering the linear stability of a unidirectional thermocapillary flow set up by a temperature gradient parallel to the free surface of an unbounded planar fluid layer. Combined, surface tension and buoyancy-driven convection in a rectangular cavity has been investigated by Rudraiah et al. [35] and the oscillatory Marangoni convection in a vertical magnetic field by Hashim and Arifin [36].

Due to the inherent complexity of MHD Marangoni convective flows, none of the above references attempted to obtain exact analytical solutions for such flows. The present work focuses on the exact analytical solution for thermosolutal MHD Marangoni boundary layers due to imposed temperature and concentration gradients in the presence of a constant magnetic field. The analysis assumes that the surface tension varies linearly with temperature and concentration but the wall temperature and concentration variations are quadratic functions of the interface arc length. In addition, the magnetic Reynolds number is assumed small and the induced magnetic field is neglected.

2. Problem formulation and governing equations

Consider steady laminar thermosolutal Marangoni boundary layer flow of a viscous, Newtonian and electrically-conducting fluid in the presence of a transverse magnetic field. The magnetic field is assumed to be of uniform strength and the magnetic Reynolds number is assumed to be small, so that the induced magnetic field is neglected. In addition, no electric field is assumed to exist, and the Hall effect is negligible. In the absence of an electric field, the small magnetic Reynolds number assumption uncouples Maxwell's equations from the Navier–Stokes equations (see Cramer and Pai [37]). The interface temperature and concentration are assumed to be quadratic functions of the distance x along the interface. The latter assumptions guarantee the existence of similarity solutions of power-law type in the presence of a uniform transversal magnetic field. Unlike the Boussinesq effect on the body force term in buoyancy-induced flows, the Marangoni surface tension effect acts as a boundary condition on the governing equations of the flow field. The governing equations for this investigation are based on the balance laws of mass, linear momentum, energy and concentration species. Taking the above assumptions into consideration, these equations can be written in dimensional form as:

$$\frac{\partial u}{\partial x}+\frac{\partial v}{\partial y}=0 \tag{1}$$

$$u\frac{\partial u}{\partial x}+v\frac{\partial u}{\partial y}=\upsilon\frac{\partial^2 u}{\partial y^2}-\frac{B_0^2\delta_{\mathrm{el}}}{\rho}u \tag{2}$$

$$u\frac{\partial T}{\partial x}+v\frac{\partial T}{\partial y}=\alpha\frac{\partial^2 T}{\partial y^2} \tag{3}$$

$$u\frac{\partial c}{\partial x}+v\frac{\partial c}{\partial y}=D\frac{\partial^2 c}{\partial y^2} \tag{4}$$

The surface tension is assumed to depend on temperature and concentration linearly,

$$\sigma=\sigma_0\big[1-\gamma_T(T-T_\infty)-\gamma_c(c-c_\infty)\big] \tag{5}$$

where

$$\gamma_T=-\frac{1}{\sigma_0}\frac{\partial\sigma}{\partial T}\bigg|_c,\qquad \gamma_c=-\frac{1}{\sigma_0}\frac{\partial\sigma}{\partial c}\bigg|_T \tag{6}$$

denote the temperature and concentration coefficients of the surface tension, respectively.

The boundary conditions of this problem are given by

$$\mu\frac{\partial u}{\partial y}\bigg|_{y=0}=-\frac{\partial\sigma}{\partial x}\bigg|_{y=0}=\sigma_0\left(\gamma_T\frac{\partial T}{\partial x}\bigg|_{y=0}+\gamma_c\frac{\partial c}{\partial x}\bigg|_{y=0}\right) \tag{7a}$$

$$v(x,0)=0,\qquad T(x,0)=T_\infty+T_0X^2$$

$$c(x,0)=c_\infty+C_0X^2,\qquad X=x/L \tag{7b}$$

$$u(x,\infty)=0,\quad T(x,\infty)=T_\infty,\quad c(x,\infty)=c_\infty \tag{7c}$$

where L is a reference length (which will be specified below) and T_0 and C_0 are (positive or negative) dimensional constants. The coordinate system, the velocity components and the interface condition are shown in Fig. 1.

By introducing the stream function $\psi(x,y)$ through the usual definition $u=\partial\psi/\partial y$, $v=-\partial\psi/\partial x$ as well as the similarity transformations,

$$\begin{aligned}&\psi(x,y)=\upsilon Xf(\eta)\\&\eta=y/L\\&T(x,y)=T_\infty+T_0X^2\theta(\eta)\\&c(x,y)=c_\infty+C_0X^2C(\eta)\end{aligned} \tag{8}$$

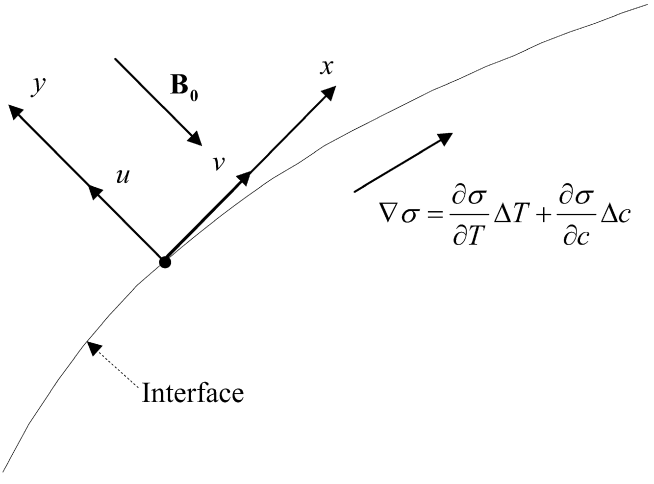

Fig. 1. Physical model, coordinate system and interface condition to a passive gas.

the boundary value problem (1)–(7) reduces to the solution of the ordinary differential equations

$$f''' + ff'' - f'^2 - Mf' = 0 \tag{9}$$

$$\frac{\theta''}{Pr} + f\theta' - 2f'\theta = 0 \tag{10}$$

$$\frac{C''}{Sc} + fC' - 2f'C = 0 \tag{11}$$

along with the boundary conditions

$$\begin{array}{l} f(0)=0, \quad f''(0)=-2(1+r), \quad \theta(0)=1, \quad C(0)=1 \\ f'(\infty)=0, \quad \theta(\infty)=0, \quad C(\infty)=0 \end{array} \tag{12}$$

In the above equations the primes denote differentiation with respect to η, r stands for the dimensionless parameter

$$r = \frac{C_0\gamma_c}{T_0\gamma_T} \tag{13}$$

and $Pr = \upsilon/\alpha$, $Sc = \upsilon/D$ and $M = B_0^2L^2\delta_{\mathrm{el}}/\mu$ denote the Prandtl number, Schmidt number and the square of the Hartmann number $H = B_0L\sqrt{\delta_{\mathrm{el}}/\mu}$, respectively. The reference length L has been chosen as

$$L = -\frac{\mu\upsilon}{\sigma_0 T_0\gamma_T} \tag{14}$$

Having in view that with increasing temperature the surface tension σ in general decreases, its temperature gradient γ_T given by Eq. (6) is positive. Thus, the reference length chosen according to Eq. (14) is positive only if T_0 is negative (see also [9]). We also mention that the parameter r represents precisely the ratio of the solutal and thermal Marangoni numbers $Ma_C = \sigma_0\gamma_C C_0 L/(\alpha\mu)$ and $Ma_T = \sigma_0\gamma_T T_0 L/(\alpha\mu)$, respectively, $r = Ma_C/Ma_T$.

Eqs. (9)–(12) show that the f-boundary value problem is decoupled from the temperature and concentration boundary value problems. Its solution $f = f(\eta)$ (see Section 3) yields the dimensional velocity field in the form

$$u(x,y) = \frac{\upsilon}{L}Xf'(\eta), \qquad v(x,y) = -\frac{\upsilon}{L}f(\eta) \tag{15}$$

The local mass flow in the boundary layer per unit span is given by:

$$\dot{m} = \rho\int_0^\infty u\,\mathrm{d}y = \rho\upsilon f(\infty)X \tag{16}$$

where $f(\infty)$ represents the similar entrainment velocity, $f(\infty) = -(L/\upsilon)v(x,\infty)$. In this way we obtain

$$\dot{m} = -\rho x v(x,\infty) \tag{17}$$

The aim of the present paper is (i) to show that the problem (9)–(12) admits exact analytical solutions for all three dimensionless functions $f(\eta)$, $\theta(\eta)$ and $C(\eta)$, and (ii) to discuss the features of these solutions in terms of the parameters Pr, Sc, M and $r = Ma_C/Ma_T$ in some detail.

3. Exact solutions of the flow problem

The momentum boundary value problem is specified by the equation

$$f''' + ff'' - f'^2 - Mf' = 0 \tag{18}$$

and the boundary conditions

$$f(0)=0, \quad f''(0)=-2(1+r), \quad f'(\infty)=0 \tag{19}$$

The function

$$f(\eta) = f_\infty(1-\mathrm{e}^{-a\eta}) \tag{20}$$

yields an exact solution of Eq. (18) when for the constants f_∞ and a the relationship

$$f_\infty = a - \frac{M}{a} \tag{21}$$

holds. The boundary condition $f(0)=0$ is satisfied automatically, the asymptotic condition $f'(\infty)=0$ requires $a>0$, and thus $f_\infty = f(\infty)$. Furthermore, the interface condition $f''(0) = -2(1+r)$ requires

$$f_\infty a^2 = 2(1+r) \tag{22}$$

Eqs. (21) and (22) lead to the cubic equation

$$a^3 - Ma - 2(1+r) = 0 \tag{23}$$

which determines the value of a for specified values of the input parameters M and r.

Then, the similar surface velocity results as

$$f'(0) = af_\infty = \frac{2(1+r)}{a} = a^2 - M \tag{24}$$

The three roots of Eq. (23) can be calculated exactly from Cardano's equations which in the present case become

$$\begin{array}{l} a_1 = s_1 + s_2 \\ a_2 = -\dfrac{s_1+s_2}{2} + \dfrac{\mathrm{i}\sqrt{3}}{2}(s_1 - s_2) \\ a_3 = -\dfrac{s_1+s_2}{2} - \dfrac{\mathrm{i}\sqrt{3}}{2}(s_1 - s_2) \end{array} \tag{25}$$

where

$$s_1 = \sqrt[3]{1+r+\sqrt{\Delta}}, \qquad s_2 = \sqrt[3]{1+r-\sqrt{\Delta}} \tag{26}$$

and

$$\Delta = (1+r)^2 - \left(\frac{M}{3}\right)^3 \tag{27}$$

As it is well known, the cubic equation admits a single real root for $\Delta > 0$ and three real roots for $\Delta \leqslant 0$, such that for $\Delta = 0$ at least two of them are coincident. The discriminate (27) vanishes when

$$M = 3(1+r)^{2/3} \tag{28}$$

the corresponding solutions being

$$a_1 = 2(1+r)^{1/3}, \quad a_2 = a_3 = -(1+r)^{1/3} \quad (\Delta = 0) \tag{29}$$

The curves of Fig. 2 represent the plots of Eq. (28) and specify the nature of solutions of the cubic equation (23) in the parameter plane (r, M). For parameter values (r, M) below these

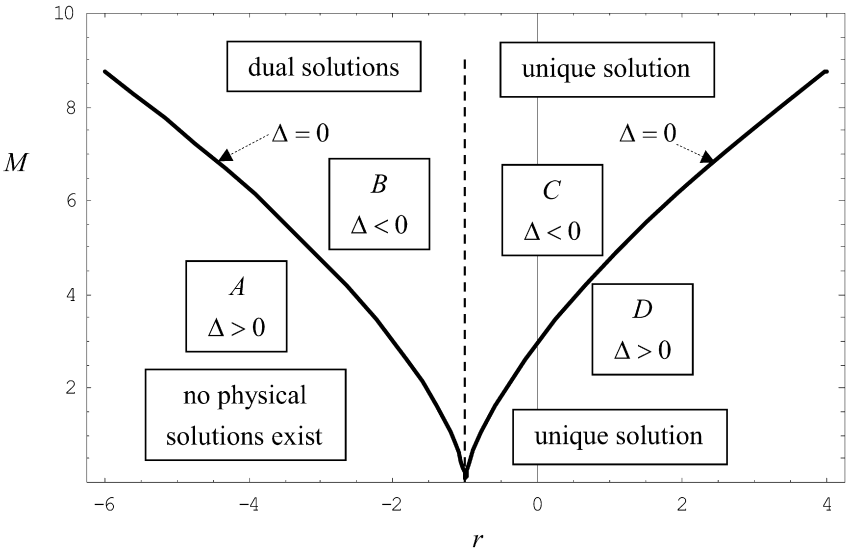

Fig. 2. The curves are the plots of Eq. (28) for which the discriminant Δ vanishes. The dashed vertical line corresponds to $r = Ma_C/Ma_T = -1$. In domain A no physical (i.e. real and positive) roots of the cubic equation (23) exist. In the domains C and D, as well as on the right branch of the $\Delta = 0$-curve, a single physical root is possible, while in the domain B two physical solutions exist which on the left branch of the $\Delta = 0$-curve become coincident.

curves, where $\Delta > 0$ (domains A and D), Eq. (23) admits at most one real solution, while above the curves of Fig. 2, where $\Delta < 0$ (domains B and C), all three roots $\{a_1, a_2, a_3\}$ are real.

Between the roots $\{a_1, a_2, a_3\}$ and the coefficients of Eq. (23) the following relationships hold

$$\begin{aligned} &a_1 + a_2 + a_3 = 0 \\ &a_1a_2 + a_1a_3 + a_2a_3 = -M \\ &a_1a_2a_3 = 2(1 + r) \end{aligned} \tag{30a-c}$$

Eq. (30a) shows that it is not possible that in the domains B and C all three roots $\{a_1, a_2, a_3\}$ are simultaneously positive or negative. Therefore, we can obtain at most two physical (i.e. positive) solutions for given values of the parameters M and r. Furthermore, Eq. (30c) shows that

(i) For $\Delta > 0$ the single real root is positive when $r > -1$ (domain D), and negative when $r < -1$ (domain A). This means that in domain D a unique physical solution exists, while in domain A no physical solution exists at all.
(ii) for $\Delta \leqslant 0$ we have two positive real roots and one negative real root when $r < -1$ (domain B and the left branch of the $\Delta = 0$ curve) and two negative real roots and one positive real root when $r > -1$ (domain C and the right branch of the $\Delta = 0$ curve). This means that in domain B dual physical solution exists, while in domain A a unique physical solution exists.

The real roots $\{a_1, a_2, a_3\}$ undergo a subtle change with the variation of the parameters M and r. This phenomenon is illustrated in Fig. 3 for $-4 < r < +2$ and $M = 3$, and $M = 6$, respectively. In the range

$$-\left(1 + (M/3)^{3/2}\right) < r < -1 \tag{31}$$

the f-boundary value problem admits dual solutions which become coincident at the lower end of interval (31). In the range $r > -1$ the solution is unique for any specified value of $M > 0$, and corresponds to the upper branch of the curves shown in Fig. 3.

The trajectories of the roots $\{a_1, a_2, a_3\}$ shown in Fig. 3 also lead to certain trajectories of the similar surface velocity $f'(0)$ given by Eq. (24). This correlation is illustrated in Fig. 4 where the trajectories of the similar interface velocities $\{f_1'(0), f_2'(0), f_3'(0)\} \equiv \{f_{01}', f_{02}', f_{03}'\}$ associated with the roots $\{a_1, a_2, a_3\}$ are plotted for $M = 3$ and $-4 < r < +2$. The surface velocities are physical in the ranges where the corresponding roots are positive (compare Fig. 4 to Fig. 3). The dashed parts of the curves are non-physical.

The similar velocity $f'(\eta)$ is according to Eqs. (20) and (22) a simple exponential function of η,

$$f'(\eta) = \frac{2(1 + r)}{a} \mathrm{e}^{-a\eta} = f'(0)\mathrm{e}^{-a\eta} \tag{32}$$

for all values of M and r. Thus, for the case of physical roots $a > 0$, one has $f'(\eta) > 0$ for $r > -1$ and $f'(\eta) < 0$ for $r < -1$, which is also clearly seen in Fig. 4. Furthermore, the thickness of the similar velocity boundary layer (32) is given by

$$\delta = \frac{2 \ln 10}{a} \tag{33}$$

where a is one of the positive roots (25), and it is a function the Hartmann number M and of the ratio r of the Marangoni numbers, $a = a(M, r)$.

The behaviour of δ for fixed r and small and large values of M is given (e.g. for $a = a_1$) by equations

$$\delta \sim \frac{2^{2/3} \ln 10}{(1 + r)^{1/3}} \left[1 - \frac{M}{3 \cdot 2^{2/3}(1 + r)^{2/3}} + \frac{M^2}{9 \cdot 2^{4/3}(1 + r)^{4/3}} - \cdots\right] \quad (M \ll 1) \tag{34}$$

and

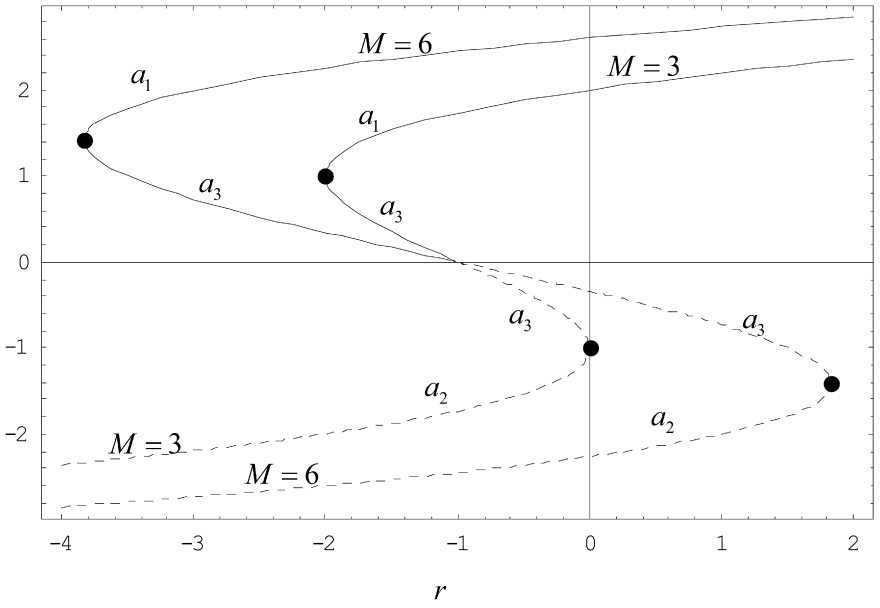

Fig. 3. Trajectories of the roots $\{a_1, a_2, a_3\}$ for $M = 3$ and $M = 6$ when r varies from -4 to $+2$. Only the positive values of a's (solid curves) correspond to physical solutions of the flow boundary value problem (18), (19).

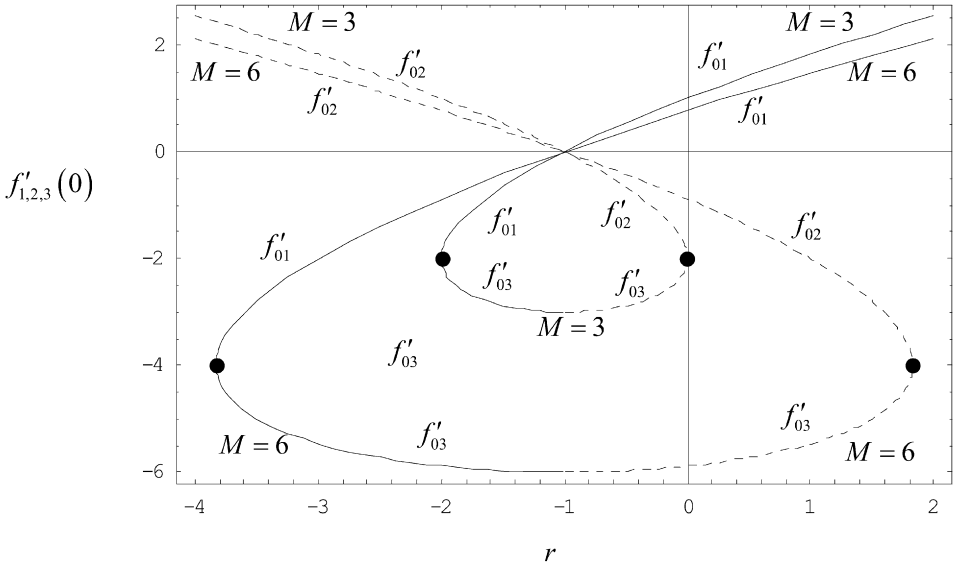

Fig. 4. Trajectories of the similar interface velocities $\{f_1'(0), f_2'(0), f_3'(0)\} \equiv \{f_{01}', f_{02}', f_{03}'\}$ associated with the roots $\{a_1, a_2, a_3\}$ shown in Fig. 3, as being plotted for $M = 3$, $M = 6$ and $-4 < r < +2$. The solid curves correspond to the physical (positive) and the dashed ones to the non-physical (negative) roots $\{a_1, a_2, a_3\}$ of the cubic equation (23).

$$\delta = \frac{2\ln 10}{\sqrt{M}}\left[1 - \frac{1+r}{M^{3/2}} + \frac{5}{2}\frac{(1+r)^2}{M^3} - 8\frac{(1+r)^3}{M^{9/2}} + \cdots\right] \quad (M \gg 1) \tag{35}$$

respectively. The full dependence of $\delta = (2\ln 10)/a_1$ on M is illustrated in Fig. 5 for three different values of the ratio $r = Ma_C/Ma_T$ of Marangoni numbers. Now it is clearly seen that, to the leading order in M, the thickness δ is independent of M, $\delta \to (2^{2/3}\ln 10)(1+r)^{-1/3}$ for $M \to 0$ and decreases as $(1+r)^{-1/3}$ with increasing values of $r > -1$. For $M \gg 1$ on the other hand, δ is, to the leading order in M, independent of r and decreases with increasing values of M as $M^{-1/2}$.

4. Exact solutions of the temperature problem

The temperature boundary value problem is specified by Eq. (10) and the corresponding θ-boundary conditions (12). Having in mind the exact flow solution (20), the θ-problem can be written in the form

$$\theta'' + ap\left[(1 - \mathrm{e}^{-a\eta})\theta' - 2a\mathrm{e}^{-a\eta}\theta\right] = 0 \tag{36}$$

$$\theta(0) = 1, \quad \theta(\infty) = 0 \tag{37}$$

where

$$p \equiv \frac{f_\infty}{a}Pr = \frac{a^2 - M}{a^2}Pr = \frac{2(1+r)}{a^3}Pr \tag{38}$$

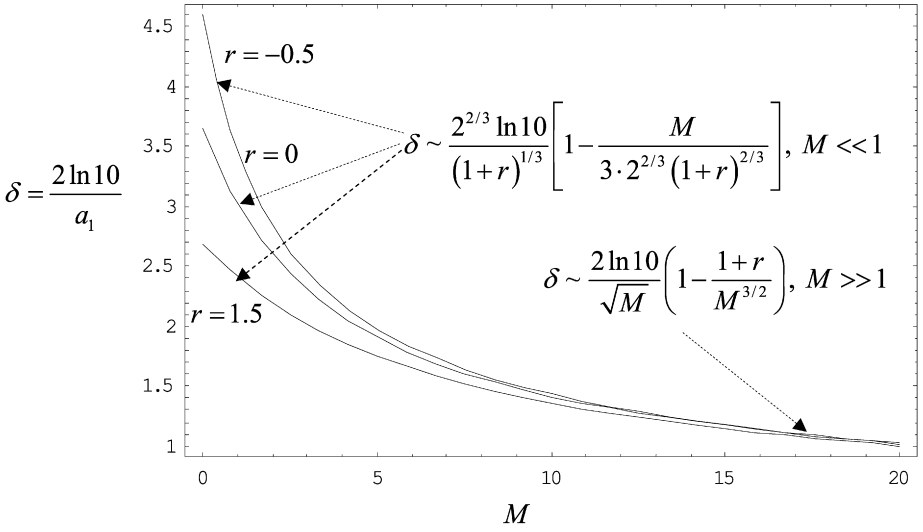

Fig. 5. Plot of the thickness $\delta = (2\ln 10)/a_1$ of the similar velocity boundary layer as a function of M for the values $r = -0.5$, 0 and 1.5 of the ratio r of Marangoni numbers.

Two exact elementary solutions of the problem (36), (37) corresponding to the special values 1 and 2 of the parameter p can easily be found. They are

$$\theta(\eta) = \frac{1}{3}(2 + \mathrm{e}^{-a\eta})\mathrm{e}^{-a\eta} \quad (p = 1) \tag{39}$$

and

$$\theta(\eta) = \mathrm{e}^{-2a\eta} \quad (p = 2) \tag{40}$$

the corresponding (dimensionless) interface temperature gradients being $\theta'(0) = -4a/3$ and $\theta'(0) = -2a$, respectively.

The forms of Eq. (36), as well as of the special solutions (39) and (40) suggest that for arbitrary values of the parameter p the change of the independent variable

$$z = z_0\mathrm{e}^{-a\eta} \tag{41}$$

can be of advantage. Indeed, by doing so, and choosing

$$z_0 = -p \tag{42}$$

our Eq. (36) reduces to

$$z\frac{\mathrm{d}^2\theta}{\mathrm{d}z^2} + (1 - p - z)\frac{\mathrm{d}\theta}{\mathrm{d}z} + 2\theta = 0 \tag{43}$$

Eq. (43) has the form of Kummer's equation of the confluent hypergeometric functions (see e.g. Abramowitz and Stegun [38], Chapt. 13). Accordingly, its solution satisfying the first boundary condition (37) is

$$\theta(\eta) = \left(\frac{z}{z_0}\right)^p \frac{{}_1F_1(p-2, p+1, z)}{{}_1F_1(p-2, p+1, z_0)} \tag{44}$$

where ${}_1F_1$ denotes Kummer's confluent hypergeometric function (see Abramowitz and Stegun [38], Chapt. 13).

Having in mind that ${}_1F_1(-1, 2, z) = 1 - (z/2)$ and ${}_1F_1(0, 3, z) = 1$, from Eq. (44) one easily recovers the special solutions (39) and (40) corresponding to $p = 1$ and $p = 2$, respectively. Moreover, taking into account the asymptotic behaviour of ${}_1F_1$ (see Abramowitz and Stegun [38], Chapt. 13), it can be shown that the boundary condition $\theta(\infty) = 0$ can only be satisfied for positive values of the parameter p. Thus, Eq. (38) implies

$$M < a^2 \tag{45}$$

In addition to $M < a^2$, the condition $p > 0$ along with $a > 0$ also requires

$$r = \frac{Ma_C}{Ma_T} > -1 \tag{46}$$

Therefore, the inequalities (45) and (46) specify the existence domain of temperature solutions of the present problem. Having in mind also Eq. (24), we may conclude that the physical solutions of both the flow and temperature boundary value problems correspond to the positive values of the dimensionless interface velocity,

$$f'(0) > 0 \quad \text{(physical solutions)} \tag{47}$$

Under these conditions, the dimensionless temperature gradient $\theta'(0)$ (which represents at the same time the dimensionless heat flux) across the interface is obtained from Eq. (44) in the form

$$\theta'(0) = -ap\left[1 - \frac{p-2}{p+1}\frac{{}_1F_1(p-1, p+2, -p)}{{}_1F_1(p-2, p+1, -p)}\right] \tag{48}$$

For small and large values of the Prandtl number the interface heat flux (48) scales with Pr and $Pr^{1/2}$, respectively, according to the relationships

$$\theta'(0) = -3f_\infty Pr \quad (Pr \to 0) \tag{49}$$

$$\theta'(0) = -1.59\sqrt{af_\infty}\cdot Pr^{1/2} \quad (Pr \to \infty) \tag{50}$$

As an illustration, in Figs. 6 and 7 the Prandtl number dependence of the interface heat flux (48) and a few temperature profiles (44) are shown for specified values of the problem parameters, respectively. As expected based on Fig. 6, the temperature profiles of Fig. 7 become steeper and steeper with increasing values of Pr.

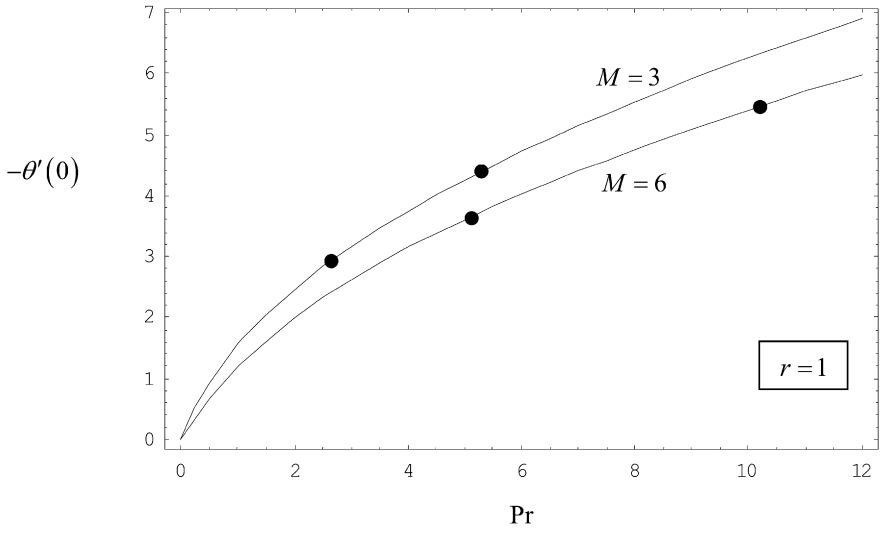

Fig. 6. Dependence on the Prandtl number of the (negative) interface heat flux (48) for $r=1$ and $M=3$ and $M=6$, respectively. The corresponding (physical) roots of the cubic equation (23) are $a_1=2.195823$ and $a_1=2.732051$, respectively. The dots correspond to the special cases (39) and (40) taken for $M=3$ and $M=6$, respectively. The small and large Pr-behavior is given by the linear and square root law (49) and (50), respectively.

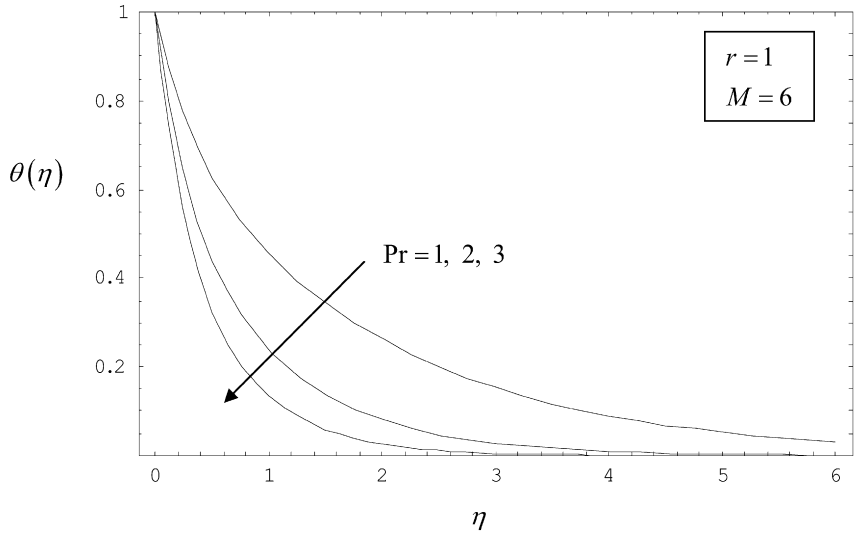

Fig. 7. Temperature profiles (44) corresponding to the parameter values $r=1$, $M=6$, and three different values of the Prandtl number.

5. Exact solutions of the concentration problem

Having in mind the exact flow solution (20), the concentration problem specified by Eq. (11) and the corresponding C-boundary conditions (12) can be written in the form

$$C''+as\left[(1-\mathrm{e}^{-a\eta})C'-2a\mathrm{e}^{-a\eta}C\right]=0 \tag{51}$$

$$C(0)=1,\quad C(\infty)=0 \tag{52}$$

where

$$s\equiv\frac{f_\infty}{a}Sc=\frac{a^2-M}{a^2}Sc=\frac{2(1+r)}{a^3}Sc \tag{53}$$

Thus, the present concentration problem is formally identical with the temperature problem specified by Eqs. (36)–(38). Accordingly, all the results of θ-problem can immediately be transcribed for the C-problem replacing θ, Pr and p by C, Sc and s, respectively.

6. Summary and conclusions

Exact analytical solutions for the velocity, temperature and concentration fields of steady thermosolutal MHD Marangoni convection have been reported in this paper. The dependence of the solutions on the parameters $r=Ma_C/Ma_T$ (ratio of the solutal and thermal Marangoni numbers), M (square of the Hartman number), Prandtl number Pr and Schmidt number Sc has been examined in some detail. The main results of the paper can be summarized as follows.

1. The flow solutions depend only on the parameters r and M. Their domain of existence in the parameter plane (r, M) is shown in Fig. 2.
2. Depending on the values of r and M there may exist either unique or dual flow solutions associated with *positive* roots a of the cubic equation (23) (see Figs. 2 and 3).

3. The similar interface velocities $f'(0)$ depend on r and M f_∞ sensitively (see Fig. 4).
4. For a given solution of the flow problem and a specified value of Pr, the temperature problem admits solutions only in the domain $\{r = Ma_C/Ma_T > -1, M < a^2\}$ of the parameter plane (r, M). Hence, according to Eq. (24), the physical solutions of both the flow and temperature boundary value problems correspond to the positive values of the dimensionless interface velocity $f'(0)$. The temperature solutions are unique and can be expressed in terms of Kummer's confluent hypergeometric functions. The characteristics of these solutions have been discussed in Section 4 in detail (see Fig. 7 for illustration).
5. To the leading order in M, the thickness δ of the similar velocity boundary layer is independent of M and decreases as $(1 + r)^{-1/3}$ with increasing values of $r > -1$. For $M \gg 1$ on the other hand, δ is, to the leading order in M, independent of r and decreases with increasing values of M as $M^{-1/2}$ (see Eqs. (34) and (35) and Fig. 5).
6. The interface heat transfer coefficient $\theta'(0)$ could also be calculated exactly [see Eq. (48)]. For small and large values of the Prandtl number, its scales with Pr and $Pr^{1/2}$, respectively (see Eqs. (49), (50) and Fig. 6).
7. The solutions of the concentration boundary value problem can be obtained by a simple transcription of the temperature solutions (see Section 5).

References

[1] L.G. Napolitano, Microgravity Fluid Dynamics, in: 2nd Levitch Conference, Washington, 1978.

[2] L.G. Napolitano, Marangoni boundary layers, in: Proc. 3rd European Symposium on Material Science in Space, Grenoble, ESA SP-142, June 1979.

[3] D.M. Christopher, B. Wang, Prandtl number effects for Marangoni convection over a flat surface, Int. J. Thermal Sci. 40 (2001) 564–570.

[4] A. Eyer, H. Leist, R. Nitsche, Floating zone growth of silicon under microgravity in sounding rocket, J. Crystal Growth 71 (1985) 173–182.

[5] J. Straub, The role of surface tension for two phase heat and mass transfer in the absence of gravity, Exp. Thermal Fluid Sci. 9 (1994) 253–273.

[6] L.G. Napolitano, Surface and buoyancy driven free convection, Acta Astronautica 9 (1982) 199–215.

[7] L.G. Napolitano, C. Golia, Coupled Marangoni boundary layers, Acta Astronautica 8 (1981) 417–434.

[8] L.G. Napolitano, G. Russo, Similar axially symmetric Marangoni boundary layers, Acta Astronautica 11 (1984) 189–198.

[9] C. Golia, A. Viviani, Marangoni buoyant boundary layers, L'Aerotechnica Missili e Spazio 64 (1985) 29–35.

[10] C. Golia, A. Viviani, Non isobaric boundary layers related to Marangoni flows, Meccanica 21 (1986) 200–204.

[11] L.G. Napolitano, G.M. Carlomagno, P. Vigo, New classes of similar solutions for laminar free convection problems, Int. J. Heat Mass Transfer 20 (1977) 215–226.

[12] I. Pop, A. Postelnicu, T. Groşan, Thermosolutal Marangoni forced convection boundary layers, Meccanica 36 (2001) 555–571.

[13] K. Arafune, A. Hirarta, Interactive solutal and thermal Marangoni convection in a rectangular open boat, Numer. Heat Transfer Part A 34 (1998) 421–429.

[14] A. Croll, W. Muller-Sebert, R. Nitsche, The critical Marangoni number for the onset of time-dependent convection in silicon, Mater. Res. Bull. 24 (1989) 995–1004.

[15] Y. Okano, M. Itoh, A. Hirata, Natural and Marangoni convections in a two-dimensional rectangular open boat, J. Chem. Engrg. Japan 22 (1989) 275–281.

[16] K. Arafune, M. Sugiura, A. Hirata, Investigation of thermal Marangoni convection in low and high Prandtl number fluids, J. Chem. Engrg. Japan 32 (1999) 104–109.

[17] K. Arafune, A. Hirata, Thermal and solutal Marangoni convection in In–Ga–Sb system, J. Crystal Growth 197 (1999) 811–817.

[18] S. Slavtchev, S. Miladinova, Thermocapillary flow in a liquid layer at minimum in surface tension, Acta Mechanica 127 (1998) 209–224.

[19] D. Schwabe, J. Metzger, Coupling and separation of buoyant and thermocapillary convection, J. Crystal Growth 97 (1989) 23–33.

[20] L.G. Napolitano, A. Viviani, R. Savino, Double-diffusive boundary layers along vertical free surfaces, Int. J. Heat Mass Transfer 35 (1992) 1003–1025.

[21] A. Al-Mudhaf, A.J. Chamkha, Similarity solutions for MHD thermosolutal Marangoni convection over a flat surface in the presence of heat generation or absorption effects, Heat Mass Transfer 42 (2005) 112–121.

[22] E. Magyari, A.J. Chamkha, Exact analytical solutions for thermosolutal Marangoni convection in the presence of heat and mass generation or consumption, Heat Mass Transfer 43 (2007) 965–974.

[23] D. Christopher, B. Wang, Marangoni convection around a bubble in microgravity, heat transfer, in: J.S. Lee (Ed.), Proceedings of the 11th international Heat Transfer Conference, vol. 3, Taylor & Francis, Levittown, 1998, pp. 486–494.

[24] M. Hainke, J. Friedrich, D. Vizman, G. Müller, MHD effects in semiconductor crystal growth and alloy solidification, in: Proceedings of the International Scientific Colloquium, Modelling for Electromagnetic Processing, 2003, pp. 73–78.

[25] J. Baumgartl, W. Budweiser, G. Müller, G. Neumann, Studies of buoyancy driven convection in a vertical cylinder with parabolic temperature profile, J. Crystal Growth 97 (1989) 9–17.

[26] J. Baumgartl, M. Gewald, R. Rupp, J. Stierlein, G. Müller, The use of magnetic fields and microgravity in melt growth of semiconductors: A comparative study, in: Proceedings VII European Symposium on Materials and Fluid Sciences under Microgravity, ESA SP-295, pp. 47–58.

[27] J. Baumgartl, G. Müller, Calculation of the effects of magnetic field damping on fluid flow-comparison of magnetohydrodynamic models of different complexity, Microgravity Quarterly 2 (1992) 197.

[28] B. Fischer, J. Friedrich, C. Kupfer, D. Vizman, G. Müller, Experimental and numerical analysis of the influence of rotating magnetic fields on heat transport in Rayleigh Benard configurations, in: Proc. 3rd Int. Conf. on Transfer Phenomena in Magnetohydro-Dynamic & Electroconducting Flows, 1997, pp. 337–342.

[29] B. Fischer, J. Friedrich, C. Kupfer, G. Müller, D. Vizman, Experimental and numerical analysis of the influence of a rotating magnetic field on convection in Rayleigh Benard configurations, in: Transfer Phenomena in Magnetohydrodynamics and Electroconducting Flows, Kluwer, Dordrecht, 1999, pp. 279–294.

[30] J. Friedrich, Y. Lee, B. Fischer, C. Kupfer, D. Vizman, G. Müller, Experimental and numerical study of Rayleigh–Benard convection affected by a rotating magnetic field, Phys. Fluids 11 (1999) 853–861.

[31] B. Fischer, J. Friedrich, U. Hilburger, G. Müller, Systematic study of buoyant flows in vertical melt cylinders under the influence of rotating magnetic fields, in: Proc. EPM2000, 2000, pp. 497–502.

[32] L.M. Witkowski, J.S. Walker, Flow driven by Marangoni convection and rotating magnetic field in a floating-zone configuration, Magnetohydrodynamics 37 (2001) 112–118.

[33] J. Priede, G. Gerbeth, A. Thess, Theoretical Aspects of Thermocapillary Convection in Liquid Metals under Magnetic Fields Influence, Electromagnetic Processing of Materials, vol. 94, Nagoya, Japan und als Publ. bei ISIJ Japan, 1994.

[34] J. Priede, G. Gerbeth, A. Thess, Thermocapillary instabilities in liquid metals: Hartmann number versus Prandtl-number, Magnetohydrodynamics, in: Proc. Energy Transfer in MHD Flows, Conference, Aussois, France, 1994, pp. 571–580.

[35] N. Rudraiah, M. Venkatachalappa, C.K. Subbaraya, Combined surface tension and buoyancy-driven convection in a rectangular open cavity in

the presence of a magnetic field, Int. J. Non-Linear Mech. 30 (1995) 759–770.

[36] I. Hashim, N.M. Arifin, Oscillatory Marangoni convection in a conducting fluid layer with a deformable free surface in the presence of a vertical magnetic field, Acta Mechanica 164 (2003) 199–215.

[37] K.R. Cramer, S.-I. Pai, Magnetofluid Dynamics for Engineers and Applied Physicists, Scripta Publishing Company, Washington, DC, 1973.

[38] M. Abramowitz, I.A. Stegun, Handbook of Mathematical Functions, Dover, New York, 1964.